JACS
JOURNAL OF THE AMERICAN CHEMICAL SOCIETY
pubs.acs.org/JACS
Article

Tuning the Reactivity of Cofacial Porphyrin Prisms for Oxygen Reduction Using Modular Building Blocks

Matthew R. Crawley, Daoyang Zhang, Amanda N. Oldacre, Christine M. Beavers, Alan E. Friedman, and Timothy R. Cook*

Cite This: J. Am. Chem. Soc. 2021, 143, 1098−1106
Read Online

ABSTRACT: We assembled eight cofacial porphyrin prisms using MTPyP (M = Co(II) or Zn(II), TPyP = 4-tetrapyridylporphyrin) and functionalized ruthenium-based "molecular clips" using coordination-driven self-assembly. Our approach allows for the rapid synthesis of these architectures in isolated yields as high as 98% for the assembly step. Structural and reactivity studies provided a deeper understanding of the role of the building blocks on the oxygen reduction reaction (ORR). Catalytic efficacy was probed by using cyclic and hydrodynamic voltammetry on heterogeneous catalyst inks in aqueous media. The reported prisms showed outstanding selectivity (>98%) for the kinetically hindered $4e^-/4H^+$ reduction of O_2 to H_2O over the kinetically more accessible $2e^-/2H^+$ reduction to H_2O_2. Furthermore, we have demonstrated significant cofacial enhancement in the observed catalytic rate constant k_s (~5 orders of magnitude) over the mononuclear analogue. We conclude that the steric bulk of the clip plays an important role in the structural dynamics of these prisms, which in turn modulates the ORR reactivity with respect to selectivity and kinetics.

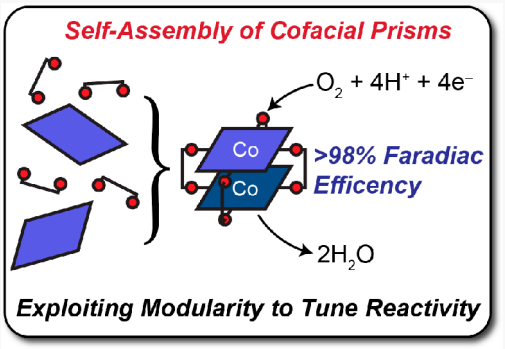

INTRODUCTION

Growing global energy consumption, in tandem with increasing initiatives to shed dependence on carbon-based fuels, has motivated the study of small-molecule activations and other energy-relevant transformations.[1] Our aim is to develop an understanding of the oxygen reduction reaction (ORR) catalyzed by polynuclear molecules with an emphasis on the factors that govern parameters such as Faradaic efficiencies, observed standard rate constants (k_s), and overpotentials (η). Much of our efforts are inspired by natural systems that necessarily use self-assembly to enforce exacting control over physical and electronic structure to influence these factors.

Many metalloenzymes feature polynuclear active sites such as the Ni−Fe sulfur cluster in carbon monoxide dehydrogenase (CODH),[2] MoFe nitrogenases,[3] and the Fe-heme/Cu-His active site of cytochrome *c* oxidase.[4] Furthermore, there is an ever-growing number of synthetic polynuclear catalysts for a variety of transformations.[5−10] Multiple metal centers allow for the spread of coordination and redox demand. This is of particular importance for small-molecule (O_2, N_2, CO_2, etc.) transformations which are often multiproton, multielectron processes. When multiple redox pathways are possible, careful control over electron and proton inventories is necessary to achieve selectivity.[11]

Over the past four decades, there has been interest in tethering multiple porphyrin groups in a cofacial, or "face-to-face", orientation. This allows for multiple metal centers to interact with one another and substrates.[12−17] Initial interest in these cofacial systems stemmed from the structural similarities to the active site in cytochrome *c* oxidase and was therefore interrogated for O_2 reduction chemistry.[14,15,18] More recently, there have been reports of cofacial porphyrin systems carrying out other small molecule activations such as CO_2 reduction.[19−21] These dinuclear catalysts have shown considerable "cofacial enhancements" on both reaction kinetics and selectivity.[15,22] Despite their impressive reactivity, cofacial porphyrin prisms have, to date, been predominantly linked through organic tethers (i.e., dibenzofuran, biphenylene, anthracene, etc.) via covalent bonds (C−C or amide bonds).[23−25] This poses a significant synthetic challenge as the porphyrin rings must be either synthesized directly off of the "clipping" group or specially designed porphyrins synthesized through complex, and oftentimes low yielding, syntheses. As a result, it is difficult to generate a library of catalysts, and consequently, there have been few systematic studies of these cofacial systems where key parameters such as

Received: November 12, 2020
Published: December 30, 2020

https://dx.doi.org/10.1021/jacs.0c11895
J. Am. Chem. Soc. 2021, 143, 1098−1106

metal−metal separation and/or electronic structure have been varied. Our lab has overcome this challenge through the use of coordination-driven self-assembly[26−35] wherein two metalloporphyrins decorated with Lewis basic donors may combine with four so-called "molecular clips" that serve as spacers. Porphyrin-based systems are particularly amenable to coordination-driven self-assembly due to their rigid structure and well-defined angularity.[9,10,14,36−40]

We hypothesized that the electron-withdrawing/donating nature of the molecular clips used in self-assembly may alter overpotentials and electron transfer rates, resulting in differences to reactivity and selectivity for ORR. Coordination-driven self-assembly is a unique and powerful way to modify distal sites since the modifications we have made to the clips do not interfere with the assembly process. In this work we report the synthesis, characterization, and study of catalytic reactivity of eight new functionalized cofacial porphyrin prisms (Figure 1). Functional groups were appended to the molecular

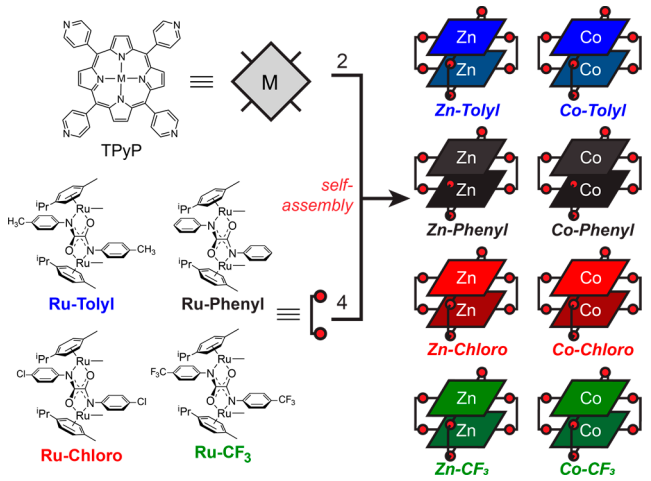

Figure 1. Modular nature of self-assembly allows for more streamlined synthesis of functionalized catalysts.

Scheme 1. Synthesis of Molecular Clips[a]

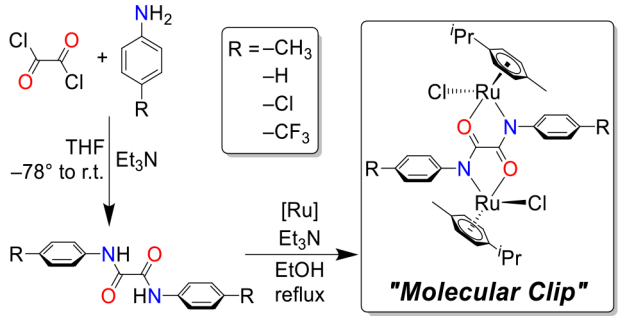

[a][Ru] = [Ru(η^6-*p*-cymene)μ^2-Cl]$_2$Cl$_2$, reflux for 24 h.

clips (Scheme 1) which were used to tether two tetra-4-pyridylporphyrin (TPyP) groups together to form the cofacial prisms. Specifically, the 4-position of *N*,*N*-phenyloxamido-bridged Ru-based clips was modified with −Me, −H, −Cl, and −CF_3 groups. To the extent that these distal changes do not significantly affect substrate access, it becomes possible to isolate the role of the clip on catalysis. Toward that end, we include an investigation of the physical structure based on X-ray diffraction and related discussions of whether molecular clips play a steric role in addition to tuning electronic structure. We emphasize that this distal tuning is enabled by coordination-driven self-assembly where we avoid the need to redesign the synthesis of each new prisms based on a conventional stepwise approach.

RESULTS AND DISCUSSION

The molecular clips used for assembly reactions were synthesized by using an adapted literature procedure as shown in ref 41. Metalation of the clips used [Ru(η^6-*p*-cymene)μ^2-Cl]$_2$Cl$_2$. The dinuclear complexes were readily isolated via recrystallization with the exception of R = −Me, in which case column chromatography was required.

Clip formation was confirmed, and purity assessed, by using a combination of ^{1}H NMR, mass spectrometry, and FT-IR spectroscopy (when discussing molecular clips, the following naming convention will be used: Ru-R group clip, e.g., Ru-CF_3 clip). In the case the Ru-CF_3 clip, single-crystal X-ray diffraction was used to determine the solid-state molecular structure (Figure 2). Further details of the syntheses, isolations, and characterizations of the molecular clips may be found in the Supporting Information.

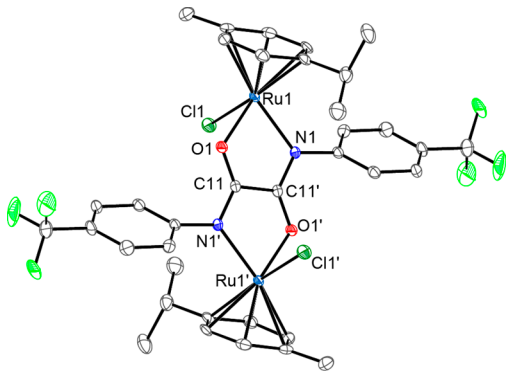

Figure 2. Solid-state structure of Ru-CF_3 clip determined by single-crystal X-ray diffraction. Thermal ellipsoids are set at the 50% probability level. Primed labels are used to denote symmetry-equivalent atoms. Hydrogen atoms and chloroform solvent molecules are omitted for clarity.

Coordination-driven self-assembly of the prisms was performed via a salt metathesis of the ruthenium molecular clip with a slight excess of silver triflate (AgOTf) and subsequent treatment with the desired porphyrin (either ZnTPyP or CoTPyP) at reflux in methanol. Although all of the prisms formed with high yields (lowest, 81%) for some combinations, the assembly process was near quantitative, with isolated yields as high as 98%. Reaction times varied—48 h for assemblies using ZnTPyP and 96 h for those using CoTPyP. This disparity is a result of the solubility differences between the two porphyrins; ZnTPyP exhibits higher solubilities in the organic solvents used as assembly media (CH_2Cl_2, acetonitrile, and methanol) than that of its cobalt counterpart. The following naming convention is used for the prisms: porphyrin metal−molecular clip−R group prism, e.g., Zn-Tolyl prism). Isolation of the green (Zn) or red (Co) self-assembled prisms was straightforward: precipitation and collection by centrifugation followed by drying *in vacuo* (see the Supporting Information for more details). Zn-based assemblies were

https://dx.doi.org/10.1021/jacs.0c11895
J. Am. Chem. Soc. 2021, 143, 1098−1106

synthesized to act as diamagnetic, catalytically inactive analogues to the Co-based assemblies for NMR and electrochemical experiments (*vide infra*).

One-dimensional NMR (^{1}H and ^{19}F{^{1}H} in the case of the Zn/Co-CF_3 prisms, see Figures S11−S19) was used for solution-state structure conformation, and diffusion ordered spectroscopy (DOSY) NMR experiments were used to rule out the formation of coordination polymers and/or smaller oligomeric species in solution. The peaks in the ^{1}H NMR spectra of the Co-porphyrin prisms were broad and showed shifts consistent with the presence of paramagnetic d^7 Co(II) centers. For the diamagnetic Zn analogues, the NMR spectra are more standard and exhibit three major regions: the first being from ∼10 to 7 ppm. Pyridyl-, pyrolic-, and aromatic oxamido-proton resonances comprise this region. Second, from ∼6.5 to 5 ppm, are the resonances from the protons of the *p*-cymene group. Finally, the aliphatic region (<3 ppm) contains the resonances of the *p*-cymene isopropyl and methyl groups as well as the methyl group of the Ru-Tolyl clip. When the spectra were integrated, the relative number of protons for each region was consistent with assemblies containing twice the number of molecular clips as porphyrins. This ratio can be narrowed down to specifically a 4 + 2 assembly by mass spectrometry, explained later. Splitting of the α- and β-protons of the pyridyl group into complex multiplets rather than sharp doublets as in the free porphyrin suggests helical chirality caused by tilting of the molecular clips, as observed by Therrien and co-workers.[37] The complex splitting pattern can be attributed to the diastereomers that may exist for these prisms, as further discussed in the crystallographic section. DOSY NMR supports the formation of uniform-sized species in solution rather than a mixture of oligomers/fragments of assembly. All peaks that were attributed to the prism were associated with the same diffusion coefficient, and each of the prisms exhibited similar diffusion coefficients. For the Zn-CF_3 prism, ^{19}F{^{1}H} NMR further affirmed assembly. The $-CF_3$ resonance shifted from the free clip (−61.98 ppm) to the assembly (−63.70 ppm). Furthermore, the peak became significantly broader, suggesting the formation of a larger molecule with slowed tumbling. The relative integrations of the triflate singlet (−79.22 ppm) to the $-CF_3$ confirms the expected 1:1 ratio.

Self-assembly stoichiometry and charge state were confirmed by electrospray ionization Fourier transform ion cyclotron resonance mass spectrometry (ESI-FT-ICR MS). Figure 3 shows the mass spectrum of the Zn-Tolyl prism as an example of the type of data obtained for these assemblies. For most prisms, the parent ion peak was either a 3+ or 4+ peak, corresponding to the intact prism which was ionized by the loss of three or four outer-sphere triflate counterions, respectively. Furthermore, in some cases the 2+ and 5+ intact prism peaks were also observed. Stoichiometry and charge state confirmation were made on the basis of the excellent agreement between the experimental mass spectrum and the simulated pattern, in terms of both isotopic intensities and charge spacings. This affirms that the desired assemblies were present in the isolated powders and persist in solution. Lower mass-to-charge ratio peaks were consistent with fragmentation of the desired assembly, that is, the $[A_3D_2 + 2OTf]^{4+}$ peak (see Figure 3) which corresponds to the loss of a single molecular clip from the assembly. In general, the same peak patterns are observed for both Zn- and Co-metalated prisms. Furthermore,

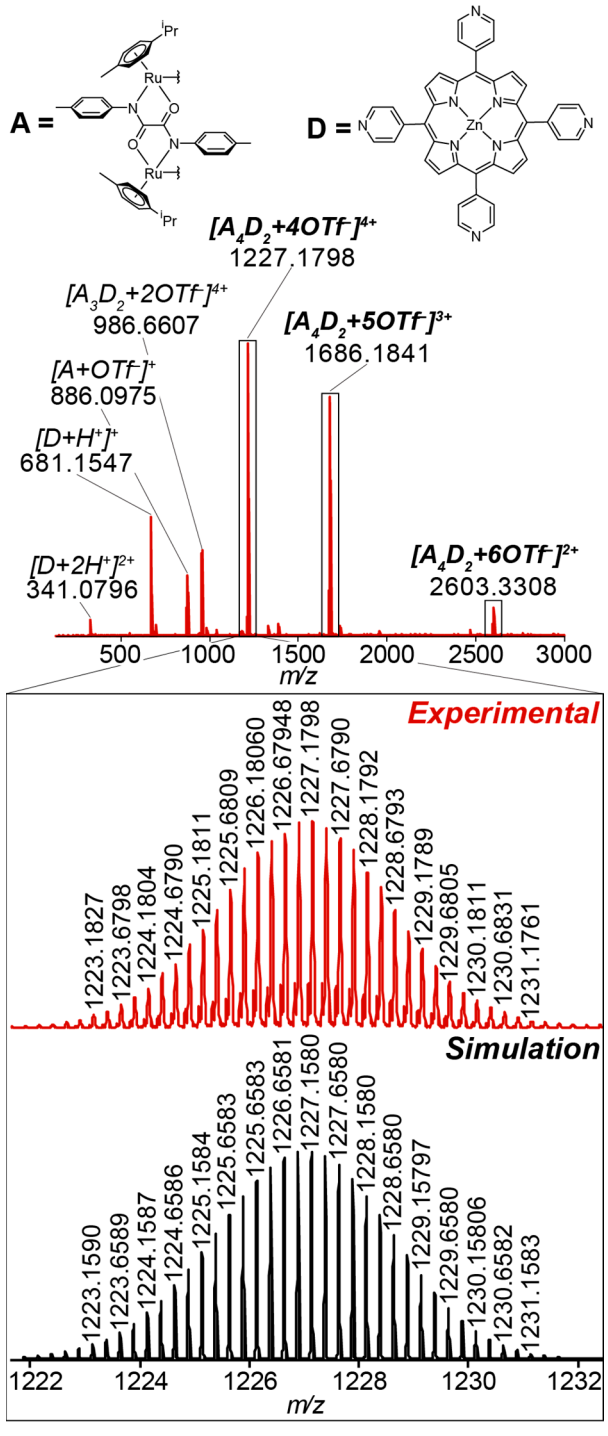

Figure 3. ESI-FT-ICR mass spectrum of the Zn-Tolyl prism. The bold peaks correspond to the intact prism. Top: full mass spectrum. Bottom: zoom in on the 4+ peak of the intact prism.

the *m*/*z* values are consistent with a Co(II) species (Supporting Information).

The vibrational spectra of the prisms are dominated by signals due to the triflate counterions at ca. 1255, 1025, and 635 cm^{-1}; these correspond to the C−F and S−O stretches and $-SO_3$ group deformation, respectively.[42] This is consistent with other reported Ru-clipped porphyrin prisms.[36] Additionally, there is no evidence of the N−H stretch associated with the starting oxamide ligand. Comparison of the Co prism to its Zn-analogue reveals near identical IR signatures, further

https://dx.doi.org/10.1021/jacs.0c11895
J. Am. Chem. Soc. 2021, 143, 1098−1106

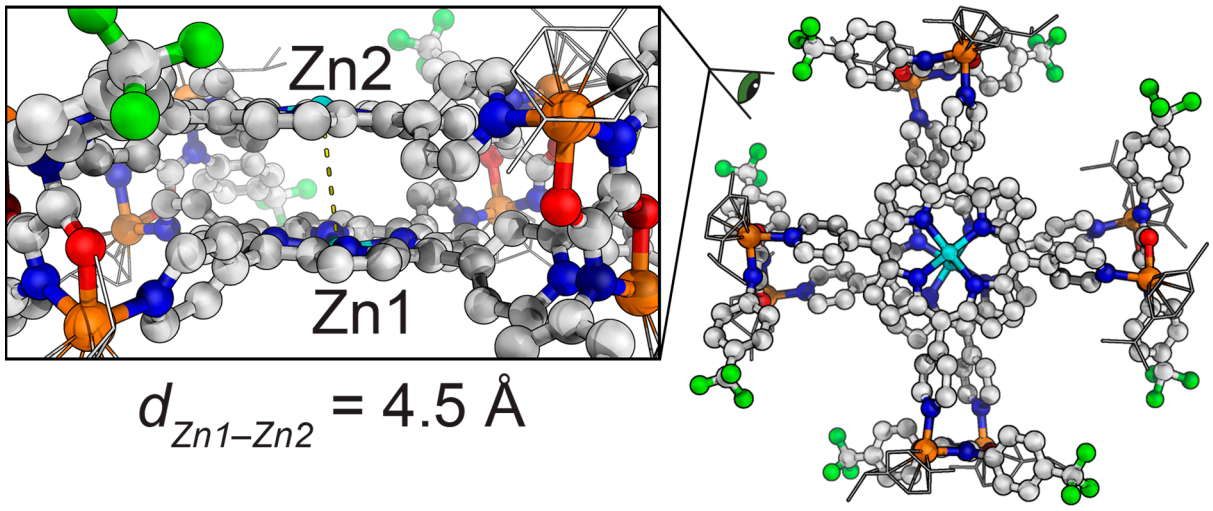

Figure 4. Crystal structure of Zn-CF_3 prism. Hydrogen atoms, axial bound water, and OTf^- counterions have been omitted for clarity.

affirming the structural similarities between the two. Electronic absorption spectroscopy reveals the expected Soret band and Q-bands, indicative of a metalated porphyrin. The Co prism Soret bands appeared around 415−420 nm, consistent with other Co(II)-porphyrin complexes in the literature (Co(III) porphyrins typical display Soret bands at ∼435−450 nm).[43,44] Examining the Q-bands, the Zn prisms exhibit two distinct, well-resolved Q-bands, while the Co prisms seem to show a single Q-band (Supporting Information). This agrees with other cobalt porphyrins in the literature and suggests the geometry at the metal center is near ideal D_{4h} point symmetry for cobalt-containing prisms and more distorted from square planar for the Zn prisms.[44]

X-ray diffraction experiments were used to confirm the molecular geometry of both the Ru-CF_3 clip and the Zn-CF_3 prism. The Ru-CF_3 clip presented the expected geometry; the two inner-sphere chloro ligands in an *anti*-configuration suggest that in solution an equilibrium between *syn*- and *anti*-geometries exists. The packing reveals a layered structure with layers of the Ru-CF_3 clip separated by cocrystallized chloroform. Crystals of the Zn-CF_3 prism were small and poorly diffracting on lab source instruments; data for the prism were collected at Berkeley National Laboratories by using the Advanced Light Source synchrotron. Diffraction beyond d_{min} of 1.00 Å was not achievable; however, the data were more than sufficient for atomic connectivity. The structure of Zn-CF_3 was easily recognized in the density map and was quite well behaved given the data quality. The *p*-cymene ligands were difficult to model, and thus their geometries were refined against coordinates produced from DFT structure optimization of free *p*-cymene (now available in Ilia's Fragment Library).[45] Careful examination of the structures reveals the stereochemical complexity associated with these architectures. First, the tilting of the molecular clip persists in the solid state. This gives rise to *M* and *P* helicity; the *M* enantiomer is shown in Figure 5. However, Zn-CF_3 crystallizes in the centrosymmetric space group *C*2/*c*, and therefore both enantiomers must exist in the crystalline phase. Once a part of the assembly, the molecular clips possess idealized C_2 point symmetry; this is purely rotational and therefore chiral. As a result, there are two orientations the clips can bind to the porphyrin (see Figure 5). Specifically, it is the relative orientations of the oxamido phenyl rings which result in these diastereomers. This leads to four

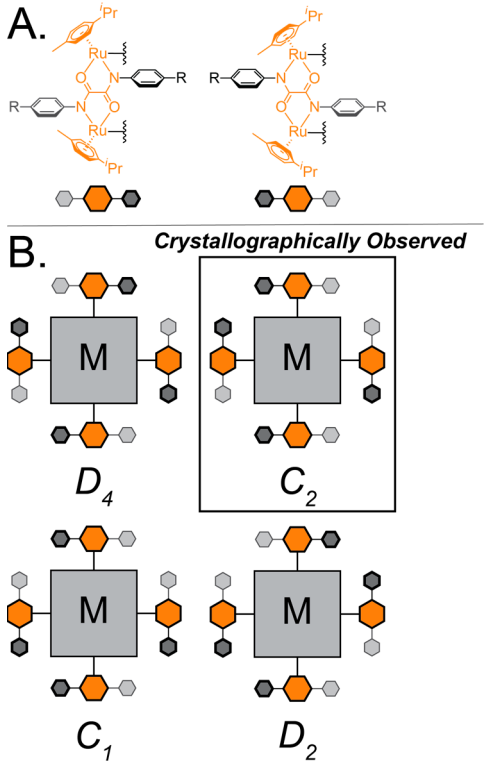

Figure 5. Symmetry analysis of conformers of functionalized cofacial porphyrin prisms. (A) The two possible orientations the molecular clip can bind to the TPyP. (B) The four possible diastereomers due to the orientation of the phenyl groups and their associated Schoenflies symbols.

possible diastereomers illustrated in Figure 5, along with the idealized symmetry of each prism. The ideal C_2 symmetric prism was crystallographically observed; there are several important consequences of this observation: First, the mixture of diastereomers explains the very complex splitting in the NMR spectra; different diastereomers will have different chemical shifts. The complexity of the observed NMR spectra suggests that all four configurations are present in solution. The relative contribution of each diastereomer is at this time unknown because of the overlap of the peaks that makes integrations nonspecific, and the factors influencing the

https://dx.doi.org/10.1021/jacs.0c11895
J. Am. Chem. Soc. 2021, 143, 1098−1106

distribution are a point of ongoing research in our lab. Variable temperature NMR spectra at 50 °C do not show substantial changes relative to those collected at room temperature (see the Supporting Information). The lack of change implies different configurations (e.g., D_4, C_2, C_1, and D_2) are not interconvertible on the NMR time scale under conditions probed, indicating that the splitting is due to the different configurations, not helical chirality. The mixture of diastereomers can also be used to rationalize the small, poorly diffracting crystals. Assuming that one diastereomer does not dominate, the effective concentration of any one will be low during crystallization, and similar diastereomers may crystallize together, leading to defects and disorder, which dramatically reduce periodicity. Nonetheless, we can extract a metal−metal separation; in this case, the Zn−Zn distance was determined to be ca. 4.5 Å. This is slightly shorter than previous self-assembled prisms but in line with the Fe−Cu separation in cytochrome *c* oxidase.[10,46] Both zinc centers were found to have an axially bound water molecule; this supports the distorted symmetry of the Zn center predicted by the Q-bands in the UV−vis spectrum. The homogeneous electrochemical behavior of the cofacial prisms was assessed by using cyclic voltammetry in acetonitrile. Under a nitrogen atmosphere, Zn- and Co-metalated prisms exhibited similar cyclic voltammograms (CVs); however, the cobalt prisms in general showed two reduction events (ca. −1 V vs $Fc^{+/0}$) before a third current response at around −1.4 V. These two events have been attributed to the two Co(II/I) couples for each of the metal centers, in agreement with other Co(II/I) couples.[47] Two distinct Co(II/I) couples imply some degree of electronic communication between the two metal centers. The remaining reductive events at ca. −1.4 V and potentials more negative are attributed to clip centered reductions (see Figure 6). The most electron-rich clip (-tolyl) shows the most negative reduction potential while the most electron-deficient clip shows the most positive.

Scanning oxidizing reveals two reversible oxidation events followed by a large irreversible wave (see the Supporting Information). These are found in both the Co- and Zn-containing prisms suggestive of ring- or clip-centered redox

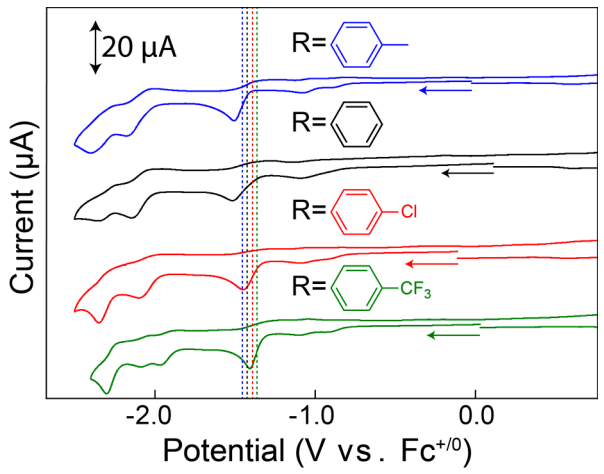

Figure 6. CV of Co prisms illustrating reductive current responses. All CVs were acquired at room temperature under a N_2 atmosphere with rigorously dry solvent. The prism concentration was 0.1 mM with 100 mM $TBAPF_6$ added as supporting electrolyte. Scan rate: 100 mV/s. Vertical lines indicate the $E_{1/2}$ value of the clip-centered reduction.

chemistry. Sparging the solution with O_2 did not lead to any appreciable change in current response within the reduced electrochemical window (reversible superoxide formation at the glassy carbon electrode limited negative potential scans). With the addition of trifluoroacetic acid (TFA) to the electrochemical cell, a large catalytic wave was observed (see Figure 7). To rule out proton reduction, a solution was sparged

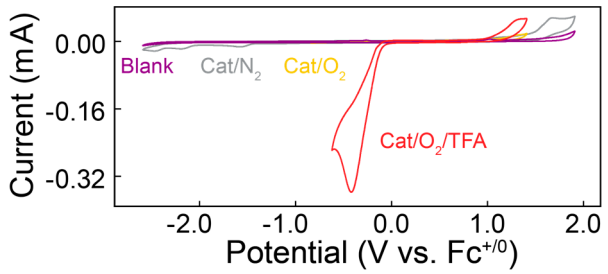

Figure 7. CV of Co-Chloro prism under variable conditions. Blank (purple, N_2 atmosphere), catalyst under inert conditions (blue, 0.1 mM Co-Chloro, N_2 atmosphere), catalyst with O_2 (red, 0.1 mM Co-Chloro, O_2 atmosphere), and catalyst under catalytic conditions (green, 0.1 mM Co-Chloro, O_2 atmosphere, 100 mM TFA). In all cases, dry acetonitrile with 100 mM $TBAPF_6$ was used.

with N_2 and TFA was added; no current response was observed at the same potential with this absence of oxygen. To confirm that catalysis occurs at the Co centers and not at the Ru clips, the same CV experiments were conducted on the Zn-analogues with no observable catalytic response. All four of the Co-containing prisms showed similar current responses at similar overpotentials (Supporting Information). To compare overpotentials, the $E_{cat/2}$ method of Appel was used.[48] The $E_{cat/2}$ values showed very little dependence on the identity of the functionalized-clip R-group, all showing a $E_{cat/2}$ of ca. −0.3 V vs $Fc^{+/0}$. Comparing the $E_{cat/2}$ values against the Hammett substituent constants does not show any apparent trend (R^2 of 0.38). Given the absence of a linear free energy relationship, we can conclude that the electronic nature of the clip does not appreciably tune the overpotentials of these prisms, though we do note that the kinetics and selectivity of these different prisms do vary significantly. To interrogate these differences without the possibility of complications due to ill-defined film formation due to adsorption, heterogeneous catalyst inks were used.

Catalyst inks of the cofacial prisms were formed by using reported methods.[10,49] Inks were then drop-cast onto a glassy carbon electrode, and the electrode was immersed in a 0.5 M H_2SO_2 aqueous solution. CV were then acquired under an inert atmosphere, which showed no current response. Upon sparging with O_2, a catalytic current response was observed (Figure 8).

Comparing the $E_{cat/2}$ values under homogeneous and heterogeneous conditions, a similar trend is observed with a trend of (positive) tolyl > chloro > phenyl ~ CF_3- (negative). We interpret this preserved trend as evidence that the electronic structure and conformation of the prisms are not significantly altered under heterogeneous conditions relative to homogeneous conditions.

To gather further insight into the parameters governing ORR, hydrodynamic voltammetric techniques were performed by using a rotating ring disk electrode (RRDE). Faradaic efficiencies for each prism were determined by comparing disk

https://dx.doi.org/10.1021/jacs.0c11895
J. Am. Chem. Soc. 2021, 143, 1098−1106

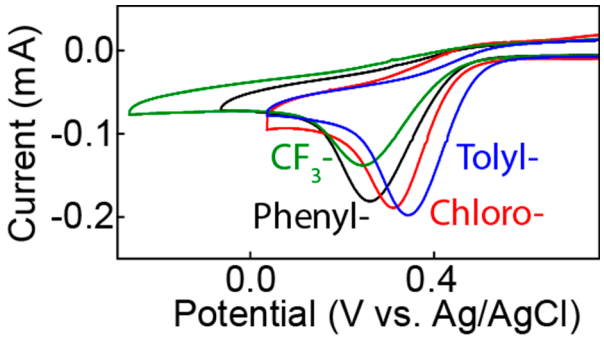

Figure 8. CV of Co-prism catalyst inks. All CV were acquired at room temperature, after the 0.5 M H_2SO_4 solution had been sparged with O_2. Scan rate: 100 mV/s.

and ring currents to determine the amount of hydrogen peroxide generated via eq 1.[10,15,50]

$$\%H_2O_2 = \frac{\frac{2i_{ring}}{N}}{i_{disk} + \frac{i_{ring}}{N}} \times 100 \quad (1)$$

where i_{ring} is the current measured at the platinum ring, i_{disk} is the current response at the modified glassy carbon disk (see Figure 9), and N is the collection efficiency of the platinum

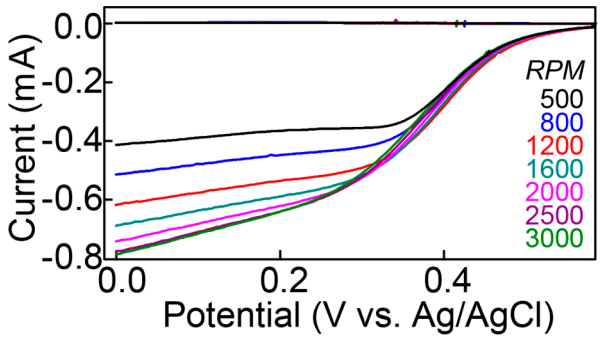

Figure 9. Hydrodynamic voltammogram of the Co-Tolyl prism using RRDE. Lower traces represent modified-disk current where catalysis is occurring (scan rate 20 mV/s); upper traces are the current response of the Pt-ring electrode held at a constant +1.0 V. Very little current response was observed at the ring electrode, suggesting high selectivity for O_2 reduction to water.

ring. The collection efficiency was experimentally determined (0.362(2)) by using the $Fe^{III/II}$ couple of potassium ferricyanide (Supporting Information).[51]

Hydrodynamic voltammetry allows for the minimization of mass-transport effects on the observed kinetics of electron transfer, enabling measurements of faradaic efficiency along with rate constants associated with electron transfer using Koutecký–Levich analysis. Tafel plots were generated to examine whether modifications to the clip lead to changes in the operative mechanism, and Koutecký–Levich analysis allowed for the determination of the standard rate constant (k_s). These results are summarized in Table 1.

There are several striking features to the data. First, the remarkable selectivity of the Co-Tolyl prisms, forming 1.6% H_2O_2 over the kinetically more challenging product, H_2O, with the remaining prisms ranging from ~3–10%. The excellent selectivity of this entire family of catalysts, ≥90% H_2O formation, is a testament to the cofacial design to favor four-

Table 1. Summary of Electrochemically Determined Catalyst Benchmarks of Co-Prism Containing Catalyst Inks

prism	$E_{cat/2}$ (V vs Ag/AgCl)	% H_2O_2	Tafel slope (mV/decade)	k_s (M^{-1} s^{-1})
Co-Tolyl	0.38(1)	1.6(1)	−130(7)	$2.2(4) \times 10^5$
Co-Phenyl	0.35(2)	3.5(3)	−101(2)	$3.4(5) \times 10^5$
Co-Chloro	0.37(2)	10.7(6)	−128(2)	$2.8(4) \times 10^5$
Co-CF_3	0.37(1)	7.5(4)	−120(3)	$9(2) \times 10^4$
CoTPyP[10]	0.16	50	−126	9.5×10^0

electron, four-proton chemistry. Under the same conditions normalized by Co concentration, CoTPyP shows 50% H_2O production. Tafel slopes for each of the prisms were all ca. 100–130 mV/decade. Similar slopes imply that there is no major shift in the operative mechanism due to different molecular clips. Rate constants for the prisms were all within an order of magnitude around 10000 times greater than that of CoTPyP, further illustrating the value of cofacial enhancements to electrocatalysts. Furthermore, the $E_{cat/2}$ values show that these catalysts operate at, or below, the overpotential measured for 10% Pt/C.[10] These cofacial prisms are among the most active ORR catalyst reported to date.

Examining all the data in concert, some fundamental conclusions regarding self-assembled cofacial catalysts may now be made. Although drastic shifts in mechanism and/or reactivity were not observed, there was modulation of said reactivity in terms of both selectivity and kinetics. These differences in reactivity were prompted by molecular changes made ~1.1 nm away from the "active sites". We were skeptical that changing the electronic structure so far away from the metals would influence catalysis, and in fact we did not observe a linear free energy relationship between Hammett parameters and overpotential under homogeneous conditions or k_s under heterogeneous conditions (Supporting Information). Because our Tafel slopes do not indicate a mechanistic shift, these observations together rule out that the changes in selectivities and rates constants are purely based on electronic effects. Instead, we surmise that variations to the clips, although occurring spatially far from the metals, impose structural ramifications on the two Co centers. We find evidence for these structural changes from our crystal data: the clip functional groups point outward, perpendicular to the Ru–pyridyl bond vector (see Figure 4). As a result, they point directly at one another and, spatially, are much closer than one may predict based on an oversimplified 2D drawing. In 3D (see Figure 5) it can be seen that the clips tilt to minimize the steric interaction between adjacent clips. The Co-Phenyl prism showed the highest rate constant followed by the Co-Tolyl and Co-Chloro prisms, which have similar sized substituents, and finally the Co-CF_3 showed the lowest rate constant, following a clean smallest-to-largest trend. It is clear that the prisms significantly break the idealized D_4 symmetric one may expect for vertical clips spanning two offset porphyrins. As the porphyrins twist, the molecular clips necessarily tilt, but because of their fixed Ru–Ru separation, the porphyrins themselves must move closer together, as illustrated in Figure 10.

Whereas our solid-state structures are a snapshot of one conformation, this twisting may be dynamic in solution, and thus the bulky R groups of the clip play a role in Co–Co separation, which explains how changes to the prisms over 1 nm away can actually impact selectivity and kinetics.

https://dx.doi.org/10.1021/jacs.0c11895
J. Am. Chem. Soc. 2021, 143, 1098–1106

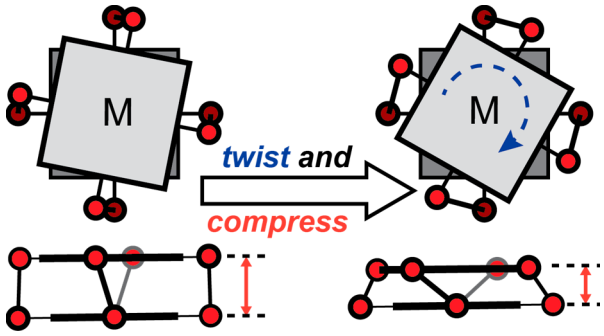

Figure 10. Modulating metal−metal separation through the canting of molecular clips.

CONCLUSIONS

We have demonstrated that coordination-driven self-assembly allows for the rapid population of a library of zinc- and cobalt-containing cofacial porphyrin prisms in three high-yielding steps. The modularity of self-assembly permitted tuning of electronic structure and steric bulk of a family of Co-based ORR electrocatalysts. Spectroscopic and solid-state characterization confirmed the anticipated cofacial porphyrin prisms were indeed synthesized assembly yields of 81−98%. Electrochemical techniques were used to probe ORR reactivity with an emphasis on correlating electronic structure to redox parameters. Kinetics and selectivities were assessed by using hydrodynamic voltammetry. Highly competitive standard rate constants were obtained by using Koutecký−Levich analysis. Tafel slopes analysis ruled out fundamental mechanistic shift between the Co prisms. Faradaic efficiencies revealed that the cofacial prisms strongly favor the four-proton, four-electron reduction to water over the kinetically more accessible two-proton, two-electron reduction to hydrogen peroxide. Substantial cofacial enhancements can been seen in all metrics of catalysis. The reported prisms even show reactivity that is comparable and, in one case, superior to Pt/C as a catalyst for ORR. Because our self-assembly approach to catalyst formation is high-yielding, rapid, and modular, we were able to make systematic changes to our prisms and establish that distal modifications can have a pronounced role in selectivity and activity. These changes arise from steric effects on the twisting of the two porphyrin faces that results in a tuning of the Co−Co distance. Efforts are underway to interrogate the solution-phase dynamics of these prisms now that we have established its importance in catalytic activity.

ASSOCIATED CONTENT

Supporting Information

The Supporting Information is available free of charge at https://pubs.acs.org/doi/10.1021/jacs.0c11895.

Synthetic procedure and spectroscopic characterization data (HR-MS, NMR, IR, UV/vis), crystallographic details, electrochemical characterization, and a detailed discussion of catalyst performance (PDF)
Crystallographic data of Ru-CF_3 (CIF)
Crystallographic data of Zn-CF_3 (CIF)

AUTHOR INFORMATION

Corresponding Author

Timothy R. Cook − *Department of Chemistry, University at Buffalo, The State University of New York, Buffalo, New York 14260, United States;* orcid.org/0000-0002-7668-8089; Email: trcook@buffalo.edu

Authors

Matthew R. Crawley − *Department of Chemistry, University at Buffalo, The State University of New York, Buffalo, New York 14260, United States;* orcid.org/0000-0002-2555-9543

Daoyang Zhang − *Department of Chemistry, University at Buffalo, The State University of New York, Buffalo, New York 14260, United States;* orcid.org/0000-0003-3722-1336

Amanda N. Oldacre − *Department of Chemistry, University at Buffalo, The State University of New York, Buffalo, New York 14260, United States;* orcid.org/0000-0001-8873-7186

Christine M. Beavers − *Advanced Light Source, Lawrence Berkeley National Laboratory, Berkeley, California 94720, United States;* orcid.org/0000-0001-8653-5513

Alan E. Friedman − *Department of Materials, Design, and Innovation, University at Buffalo, The State University of New York, Buffalo, New York 14260, United States;* orcid.org/0000-0002-4764-8168

Complete contact information is available at: https://pubs.acs.org/10.1021/jacs.0c11895

Author Contributions

M.R.C. and D.Z. contributed equally to this work.

Notes

The authors declare no competing financial interest.

ACKNOWLEDGMENTS

SC-XRD data for Zn-CF_3 were collected on the LBNL Beamline 12.2.1. This research used resources of the Advanced Light Source, which is a DOE Office of Science User Facility under Contract DE-AC02-05CH11231. The authors thank SUNY Fredonia for the use of their X-ray diffractometer. This work was supported by NSF Career Award #1847950 (T.R.C.) and a UB Silbert Fellowship (M.R.C.).

REFERENCES

(1) Lewis, N. S.; Nocera, D. G. Powering the planet: chemical challenges in solar energy utilization. *Proc. Natl. Acad. Sci. U. S. A.* **2006**, *103*, 15729−15735.
(2) Ragsdale, S. W. Metals and Their Scaffolds To Promote Difficult Enzymatic Reactions. *Chem. Rev.* **2006**, *106*, 3317−3337.
(3) Bjornsson, R.; Delgado-Jaime, M. U.; Lima, F. A.; Sippel, D.; Schlesier, J.; Weyhermüller, T.; Einsle, O.; Neese, F.; DeBeer, S. Molybdenum L-Edge XAS Spectra of MoFe Nitrogenase. *Z. Anorg. Allg. Chem.* **2015**, *641*, 65−71.
(4) Yoshikawa, S.; Shimada, A. Reaction Mechanism of Cytochrome c Oxidase. *Chem. Rev.* **2015**, *115*, 1936−1989.
(5) Hetterscheid, D. G. H.; Chikkali, S. H.; de Bruin, B.; Reek, J. N. H. Binuclear Cooperative Catalysts for the Hydrogenation and Hydroformylation of Olefins. *ChemCatChem* **2013**, *5*, 2785−2793.
(6) Tanaka, H.; Nishibayashi, Y.; Yoshizawa, K. Interplay between Theory and Experiment for Ammonia Synthesis Catalyzed by Transition Metal Complexes. *Acc. Chem. Res.* **2016**, *49*, 987−995.
(7) Trehoux, A.; Mahy, J.-P.; Avenier, F. A growing family of O2 activating dinuclear iron enzymes with key catalytic diiron(III)-peroxo intermediates: Biological systems and chemical models. *Coord. Chem. Rev.* **2016**, *322*, 142−158.
(8) Rej, S.; Tsurugi, H.; Mashima, K. Multiply-bonded dinuclear complexes of early-transition metals as minimum entities of metal cluster catalysts. *Coord. Chem. Rev.* **2018**, *355*, 223−239.

(9) Oldacre, A. N.; Friedman, A. E.; Cook, T. R. A Self-Assembled Cofacial Cobalt Porphyrin Prism for Oxygen Reduction Catalysis. *J. Am. Chem. Soc.* **2017**, *139*, 1424−1427.
(10) Oldacre, A. N.; Crawley, M. R.; Friedman, A. E.; Cook, T. R. Tuning the Activity of Heterogeneous Cofacial Cobalt Porphyrins for Oxygen Reduction Electrocatalysis through Self-Assembly. *Chem. - Eur. J.* **2018**, *24*, 10984−10987.
(11) Zhang, R.; Warren, J. J. Controlling the Oxygen Reduction Selectivity of Asymmetric Cobalt Porphyrins by Using Local Electrostatic Interactions. *J. Am. Chem. Soc.* **2020**, *142*, 13426−13434.
(12) Chang, C. K. μ-Superoxodicobalt complex of a cofacial diporphyrin. *J. Chem. Soc., Chem. Commun.* **1977**, 800−801.
(13) Collman, J. P.; Elliott, C. M.; Halbert, T. R.; Tovrog, B. S. Synthesis and characterization of "face-to-face" porphyrins. *Proc. Natl. Acad. Sci. U. S. A.* **1977**, *74*, 18−22.
(14) Collman, J. P.; Denisevich, P.; Konai, Y.; Marrocco, M.; Koval, C.; Anson, F. C. Electrode catalysis of the four-electron reduction of oxygen to water by dicobalt face-to-face porphyrins. *J. Am. Chem. Soc.* **1980**, *102*, 6027−6036.
(15) Durand, R. R.; Bencosme, C. S.; Collman, J. P.; Anson, F. C. Mechanistic aspects of the catalytic reduction of dioxygen by cofacial metalloporphyrins. *J. Am. Chem. Soc.* **1983**, *105*, 2710−2718.
(16) Chang, C. J.; Deng, Y.; Heyduk, A. F.; Chang, C. K.; Nocera, D. G. Xanthene-Bridged Cofacial Bisporphyrins. *Inorg. Chem.* **2000**, *39*, 959−966.
(17) Deng, Y.; Chang, C. J.; Nocera, D. G. Direct Observation of the "Pac-Man" Effect from Dibenzofuran-Bridged Cofacial Bisporphyrins. *J. Am. Chem. Soc.* **2000**, *122*, 410−411.
(18) Collman, J. P.; Anson, F. C.; Barnes, C. E.; Bencosme, C. S.; Geiger, T.; Evitt, E. R.; Kreh, R. P.; Meier, K.; Pettman, R. B. Further studies of the dimeric.beta.-linked "face-to-face four" porphyrin: FTF4. *J. Am. Chem. Soc.* **1983**, *105*, 2694−2699.
(19) Mohamed, E. A.; Zahran, Z. N.; Naruta, Y. Efficient electrocatalytic CO_2 reduction with a molecular cofacial iron porphyrin dimer. *Chem. Commun.* **2015**, *51*, 16900−16903.
(20) Mohamed, E. A.; Zahran, Z. N.; Naruta, Y. Efficient Heterogeneous CO_2 to CO Conversion with a Phosphonic Acid Fabricated Cofacial Iron Porphyrin Dimer. *Chem. Mater.* **2017**, *29*, 7140−7150.
(21) Zahran, Z. N.; Mohamed, E. A.; Abdel Haleem, A.; Naruta, Y. Efficient Solar-Assisted O2 Reduction Using a Cofacial Iron Porphyrin Dimer Catalyst Integrated into a p-$CuBi_2O_4$ Photocathode. *Chem. - Eur. J.* **2018**, *24*, 10606−10611.
(22) Chang, C. K.; Liu, H. Y.; Abdalmuhdi, I. Electroreduction of oxygen by pillared cobalt(II) cofacial diporphyrin catalysts. *J. Am. Chem. Soc.* **1984**, *106*, 2725−2726.
(23) Hiom, J.; Paine, J. B., III; Zapf, U.; Dolphin, D. The synthesis of cofacial porphyrin dimers. *Can. J. Chem.* **1983**, *61*, 2220−3.
(24) Le Mest, Y.; L'Her, M.; Courtot-Coupez, J.; Collman, J. P.; Evitt, E. R.; Bencosme, C. S. Electrochemical behaviour of a binary cofacial dicobalt porphyrin in aprotic media under a nitrogen atmosphere: Formation of mixed-valence compounds. *J. Electroanal. Chem. Interfacial Electrochem.* **1985**, *184*, 331−346.
(25) Kim, K.; Collman, J. P.; Ibers, J. A. Structure of the dicobalt "face-to-face" porphyrin with two four-atom amide bridges. *J. Am. Chem. Soc.* **1988**, *110*, 4242−4246.
(26) Fujita, M. Metal-directed self-assembly of two- and three-dimensional synthetic receptors. *Chem. Soc. Rev.* **1998**, *27*, 417−425.
(27) Inokuma, Y.; Arai, T.; Fujita, M. Networked molecular cages as crystalline sponges for fullerenes and other guests. *Nat. Chem.* **2010**, *2*, 780−783.
(28) Stang, P. J.; Olenyuk, B.; Fan, J.; Arif, A. M. Combining Ferrocenes and Molecular Squares: Self-Assembly of Heterobimetallic Macrocyclic Squares Incorporating Mixed Transition Metal Systems and a Main Group Element. Single-Crystal X-ray Structure of $[Pt(dppf)(H_2O)_2][OTf]_2$. *Organometallics* **1996**, *15*, 904−908.
(29) Yang, H. B.; Das, N.; Huang, F.; Hawkridge, A. M.; Muddiman, D. C.; Stang, P. J. Molecular architecture via coordination: self-assembly of nanoscale hexagonal metallodendrimers with designed building blocks. *J. Am. Chem. Soc.* **2006**, *128*, 10014−10015.
(30) Northrop, B. H.; Yang, H. B.; Stang, P. J. Coordination-driven self-assembly of functionalized supramolecular metallacycles. *Chem. Commun.* **2008**, 5896−908.
(31) Li, S.; Huang, J.; Cook, T. R.; Pollock, J. B.; Kim, H.; Chi, K.-W.; Stang, P. J. Formation of [3]Catenanes from 10 Precursors via Multicomponent Coordination-Driven Self-Assembly of Metallarectangles. *J. Am. Chem. Soc.* **2013**, *135*, 2084−2087.
(32) Mal, P.; Schultz, D.; Beyeh, K.; Rissanen, K.; Nitschke, J. R. An Unlockable−Relockable Iron Cage by Subcomponent Self-Assembly. *Angew. Chem., Int. Ed.* **2008**, *47*, 8297−8301.
(33) Roberts, D. A.; Pilgrim, B. S.; Cooper, J. D.; Ronson, T. K.; Zarra, S.; Nitschke, J. R. Post-assembly Modification of Tetrazine-Edged FeII4L6 Tetrahedra. *J. Am. Chem. Soc.* **2015**, *137*, 10068−10071.
(34) Caulder, D. L.; Brückner, C.; Powers, R. E.; König, S.; Parac, T. N.; Leary, J. A.; Raymond, K. N. Design, Formation and Properties of Tetrahedral M4L4 and M4L6 Supramolecular Clusters1. *J. Am. Chem. Soc.* **2001**, *123*, 8923−8938.
(35) Cook, T. R.; Stang, P. J. Recent Developments in the Preparation and Chemistry of Metallacycles and Metallacages via Coordination. *Chem. Rev.* **2015**, *115*, 7001−45.
(36) Barry, N. P. E.; Govindaswamy, P.; Furrer, J.; Suess-Fink, G.; Therrien, B. Organometallic boxes built from 5,10,15,20-tetra(4-pyridyl)porphyrin panels and hydroxyquinonato-bridged diruthenium clips. *Inorg. Chem. Commun.* **2008**, *11*, 1300−1303.
(37) Barry, N. P. E.; Austeri, M.; Lacour, J.; Therrien, B. Highly Efficient NMR Enantiodiscrimination of Chiral Octanuclear Metalla-Boxes in Polar Solvent. *Organometallics* **2009**, *28*, 4894−4897.
(38) Han, Y.-F.; Lin, Y.-J.; Weng, L.-H.; Berke, H.; Jin, G.-X. Stepwise formation of "organometallic boxes" with half-sandwich Ir, Rh and Ru fragments. *Chem. Commun.* **2008**, 350−352.
(39) Ward, B.; Wang, C.-B.; Chang, C. K. Nonbonding steric effect on carbon monoxide and oxygen binding to hemes. Kinetics of ligand binding in iron-copper cofacial diporphyrins and strapped hemes. *J. Am. Chem. Soc.* **1981**, *103*, 5236−5238.
(40) Collman, J. P.; Bencosme, C. S.; Durand, R. R.; Kreh, R. P.; Anson, F. C. Mixed-metal face-to-face porphyrin dimers. *J. Am. Chem. Soc.* **1983**, *105*, 2699−2703.
(41) Casellato, U.; Guerriero, P.; Tamburini, S.; Vigato, P. A. Metal complexes with disubstituted oxamidic ligands. *Inorg. Chim. Acta* **1997**, *260*, 1−9.
(42) Johnston, D. H.; Shriver, D. F. Vibrational study of the trifluoromethanesulfonate anion: unambiguous assignment of the asymmetric stretching modes. *Inorg. Chem.* **1993**, *32*, 1045−1047.
(43) Sun, H.; Smirnov, V. V.; DiMagno, S. G. Slow Electron Transfer Rates for Fluorinated Cobalt Porphyrins: Electronic and Conformational Factors Modulating Metalloporphyrin ET. *Inorg. Chem.* **2003**, *42*, 6032−6040.
(44) Lopes, J. M. S.; Sampaio, R. N.; Ito, A. S.; Batista, A. A.; Machado, A. E. H.; Araujo, P. T.; Neto, N. M. B. Evolution of electronic and vibronic transitions in metal(II) meso-tetra(4-pyridyl)-porphyrins. *Spectrochim. Acta, Part A* **2019**, *215*, 327−333.
(45) Guzei, I. An idealized molecular geometry library for refinement of poorly behaved molecular fragments with constraints. *J. Appl. Crystallogr.* **2014**, *47*, 806−809.
(46) Yoshikawa, S.; Shinzawa-Itoh, K.; Nakashima, R.; Yaono, R.; Yamashita, E.; Inoue, N.; Yao, M.; Fei, M. J.; Libeu, C. P.; Mizushima, T.; Yamaguchi, H.; Tomizaki, T.; Tsukihara, T. Redox-Coupled Crystal Structural Changes in Bovine Heart Cytochrome c Oxidase. *Science* **1998**, *280*, 1723−1729.
(47) Lacy, D. C.; McCrory, C. C. L.; Peters, J. C. Studies of Cobalt-Mediated Electrocatalytic CO_2 Reduction Using a Redox-Active Ligand. *Inorg. Chem.* **2014**, *53*, 4980−4988.
(48) Appel, A. M.; Helm, M. L. Determining the Overpotential for a Molecular Electrocatalyst. *ACS Catal.* **2014**, *4*, 630−633.
(49) Mihara, N.; Yamada, Y.; Takaya, H.; Kitagawa, Y.; Aoyama, S.; Igawa, K.; Tomooka, K.; Tanaka, K. Oxygen Reduction to Water by a

https://dx.doi.org/10.1021/jacs.0c11895
J. Am. Chem. Soc. 2021, 143, 1098−1106

Cofacial Dimer of Iron(III)−Porphyrin and Iron(III)−Phthalocyanine Linked through a Highly Flexible Fourfold Rotaxane. *Chem. - Eur. J.* **2017**, *23*, 7508−7514.
(50) Pegis, M. L.; Martin, D. J.; Wise, C. F.; Brezny, A. C.; Johnson, S. I.; Johnson, L. E.; Kumar, N.; Raugei, S.; Mayer, J. M. Mechanism of Catalytic O2 Reduction by Iron Tetraphenylporphyrin. *J. Am. Chem. Soc.* **2019**, *141*, 8315−8326.
(51) Bard, A. J.; Faulkner, L. R. *Electrochemical Methods: Fundamentals and Applications*; Wiley: 2000.

https://dx.doi.org/10.1021/jacs.0c11895
J. Am. Chem. Soc. 2021, 143, 1098−1106